Quasi-static indentation and impact in glass-fibre reinforced polymer sandwich panels for civil and ocean engineering applications

M. Garrido, R. Teixeira, J.R. Correia, L.S. Sutherland

Abstract

Sandwich structures comprising glass-fibre reinforced polymer faces and low-density core constitute an efficient and versatile constructive system for civil and ocean engineering structures. However, being multilayered with relatively soft core materials, they are particularly susceptible to damage under concentrated loads. Whilst numerous studies exist on the indentation and impact behaviour of sandwich composites, the great majority considers the thin-skinned laminates used by the aeronautical industry. To mitigate the lack of studies on the significantly thicker and more robust civil and ocean engineering sandwich laminates, the quasi-static indentation and low-velocity impact behaviour of such panels is experimentally studied. Three types of core materials (polyurethane and polyethylene terephthalate foams and end-grain balsa) and five different indenters, of varying shape (hemispherical versus flat) and diameter (10, 20 and 30 mm), are considered. Flat and larger indenters required higher loads and energies for first damage and perforation. The first damage and peak resistance values of the polyethylene terephthalate panels were, respectively, 15 and 8% higher than in the polyurethane panels; for the balsa panels, such figures were 20 and 10%. The polyurethane panels showed the highest energy absorption capacity. Predictions of first damage resistance given by two analytical models (for flat and hemispherical indenters) were assessed against the gathered experimental data. The obtained predictions were reasonably accurate, but indicate a need for further calibration, mainly concerning the effects of core material.

Keywords

Sandwich panels, civil engineering, ocean engineering, quasi-static indentation, low-velocity impact

1 Introduction

Sandwich structures comprising glass-fibre reinforced polymer (GFRP) faces and low-density core materials present high strength- and stiffness-to-weight ratios, constituting an efficient and versatile constructive system for civil engineering applications [1]. Moreover, they present multifunctional potential, being able to provide high thermal insulation or to incorporate solar cells underneath the face sheets [2,3], making sandwich construction a very interesting alternative to traditional construction materials. However, being multilayered and comprising relatively soft core materials, sandwich panels can be particularly susceptible to damage induced by concentrated loads.

Events such as tool drops during construction, pedestrians walking on high heels in footbridges and furniture supports in building floors can induce localised damage with detrimental consequences for the behaviour of the sandwich panels. The vulnerability of both monolithic

and sandwich laminated composite materials to out-of-plane impact events has been a known problem for many years, with a great deal of research carried out in this field. In fact, far too much research has been completed to be reviewed here, but this has already been done in detail elsewhere (e.g. Abrate [4–7] and Cantwell and Morton [8]). However, the great majority of this work has considered the thin-skinned, usually pre-preg carbon and often honeycomb-cored laminates used by the aeronautical industry; mostly because of the critical nature of potential weight savings and also the relative abundance of resources available in this field [9].

Although potential weight savings in the civil industry are extremely attractive, the need for far more robust structures means that far thicker skinned and overall thicker panels are used for civil engineering applications. Since the impact behaviour of composite materials is highly dependent on the many possible material parameters [9], this means that this aeronautically biased work will most likely not be applicable to other types of laminates.

Marine industry composite material applications for small to medium size vessels can be considered to be 'between' those of the aeronautical and civil fields, for example weight is not as important as in the aeronautical applications, but is more important than for most civil applications. Envisaging the respective applications of an aircraft, a fast ferry and a bridge help illustrate this concept. However, typical marine vessel composites are actually approaching those used in civil engineering in that they are generally far more robust and thicker than those used in aircraft, and glass and polyester are far more ubiquitous than carbon and epoxy. Further, once less weight sensitive marine applications are considered, for example in superstructures for offshore platforms or ships, the even thicker and thicker-skinned laminates used in civil engineering become most appropriate.

There is a lack of studies concerning indentation and impact on the significantly thicker and more robust typical civil engineering sandwich laminates, and hence this present work on such laminates, as an extension to previous work on pultruded footbridge multicellular deck panels [10,11], aims to start to remedy this severe lack of data and understanding. However, the work considering impact on similar, albeit less robust, lighter marine composites, as reviewed in Sutherland [9,12–14], can be used as a starting point for the more substantial laminates investigated here.

Studies of impact on marine composites have shown the influence of both (i) indenter/impactor geometry (e.g. Hildebrand [15], Muscat-Fenech et al. [16,17] and Sutherland and Guedes Soares [18,19] and see the review of this aspect of impact event in Sutherland [12]) and (ii) core material (e.g. Hildebrand [15], Aamlid [20], Atas and Sevim [21] and Daniel et al. [22] and see the review of this material parameter in Sutherland [12]) to be especially important, and hence the effects of these two fundamental parameters are investigated here.

The numerical modelling of the behaviour of composite sandwich panels under concentrated loads is often based on user-defined routines with failure initiation simulation of the composite skins using the Hashin criterion together with a damage progression law [23,24]. Good agreement between the experimental data and numerical models has often been achieved, but again these studies do not consider the more robust sandwich panels suitable for civil and

ocean engineering structural applications and therefore their behaviour under local and impact loads may not be comparable.

Analytical models predicting the impact behaviour of composite sandwich panels are most often based on Hertzian contact, energy balance and/or spring–mass models [5]. However, these models are only capable of describing the elastic phase of the impact behaviour and become invalid as soon as damage occurs. Analytical models proposed for the prediction of the onset of damage which may be used in the preliminary design of composite sandwich panels are still very scarce; those by Olsson [25] and Wen et al. [26] are among some of the very few examples available.

Hence, the current paper presents experimental and analytical studies of the quasi-static (QS) indentation and low-velocity impact behaviour of GFRP composite sandwich panels designed for civil and ocean engineering structural applications. Sandwich panel specimens with relatively thick GFRP faces and different core materials were tested using hemispherical and flat indenters of different diameters. The experimental results were used to assess two analytical models found in the existing literature.

2 Experimental details

The experimental study presented here aims to (i) assess the behaviour of relatively thick and thick-skinned sandwich panels, designed for structural applications in civil and ocean engineering, under QS indentation and low-velocity impact actions, and to (ii) determine the influence of core materials and indenter characteristics in such behaviour. Additionally, it is intended to evaluate the possibility of using QS tests as a simpler and less resource intensive alternative for predicting the impact response of such sandwich panels. This approach has been previously validated for monolithic and marine sandwich laminates in previous studies [27,28].

2.1 Materials, indenters and specimens

To investigate the effect of core material, three different typical materials were considered: (i) rigid polyurethane (PUR) foam; (ii) polyethylene terephthalate (PET) foam and (iii) end-grain balsa (BAL). The sandwich facings were identical for all panel types, consisting of vacuum infused GFRP laminates produced on the core material itself, automatically guaranteeing the bond between the faces and core and thus avoiding the need for additional adhesives. A symmetrical $[0/0/30/–30/90/0]_S$ layup of unidirectional E-glass fibres in an orthophthalic polyester resin was used. The panels were of total thickness 134 mm, with 7 mm thick faces separated by a 120 mm thick core (Figure 1). The relevant mechanical and physical properties of the core materials and GFRP laminates, determined previously [29], are presented in Tables 1and 2, including (core material and laminate) density (ρ), tensile strength (σ_{tu}), compressive strength (σ_{cu}), shear strength (τ_u), elasticity moduli (E), shear modulus (G) and (laminate) Poisson ratios (ν) and interlaminar shear strength (τ_{isu}), where the subscripts L and T refer to longitudinal and transverse directions.

Figure 1. Cross-section of the sandwich panels; left to right: PUR foam, PET foam, balsa wood.

Material	ρ(kg/m^3)	σ_{tu}[a] (MPa)	σ_{cu}[a] (MPa)	τ_u (MPa)	G[b] (MPa)
PUR foam	87.4	0.68	0.64	0.32	8.7
PET foam	105.4	1.03	1.32	0.94	19.2
End-grain balsa	101.4	4.26	5.76	0.93	48.8

[a]Determined along the through-thickness direction of the panels.
[b]Determined for the shear plane defined by the panel longitudinal and through-thickness directions.

Table 1. Core material mechanical properties [29].

$\sigma_{tu,L}$ (MPa)	$E_{t,L}$ (GPa)	$\sigma_{tu,T}$ (MPa)	$E_{t,T}$ (GPa)	$\sigma_{tu,L}$ (MPa)	$\sigma_{cu,T}$ (MPa)	$\tau_{u,LT}$ (MPa)	G_{LT} (GPa)	ν_{LT} (–)	ν_{TL} (–)	$\tau_{isu,L}$ (MPa)	$\tau_{isu,T}$ (MPa)
437.3	29.4	179.6	15.6	249.8	194.2	49.4	4.1	0.31	0.17	37.1	24.1

Table 2. GFRP laminate mechanical properties [29].

In order to explore a significant range of indenter geometries, five different stainless steel indenters were used (Figure 2), namely two flat-ended indenters with diameters of 10 and 20 mm (10F and 20F), and three hemispherical-ended indenters with diameters of 10, 20 and 30 mm (10H, 20H and 30H).

Figure 2. Flat and hemispherical indenters.

2.2 Test equipment and instrumentation

2.2.1 QS indentation tests

The QS indentation tests were performed on an Instron 1343universal test machine with a load capacity of 250 kN and an integrated load cell with the same capacity and 0.01 kN precision (Figure 3(a)). The selection of specimen size is discussed in the 'Experimental programme' section, and specimens were fully supported by a rigid 50 mm thick steel plate. The concentrated load was applied at the centre of the sandwich panels by the indenters at a speed of 2 mm/min. Two displacement transducers (TML CDP-25, 25 mm stroke and 0.01 mm precision) were used to measure the vertical deflections at two different points along the longitudinal and transverse directions of the upper face sheet laminates (Figure 3(b)). These measurement points were located 50 mm away from the loading point, with the exception of the slightly larger PUR foam cored specimens loaded with 20 and 30 mm indenters, for which a distance of 75 mm was adopted owing to the higher deformability of this core material (Figure 4).

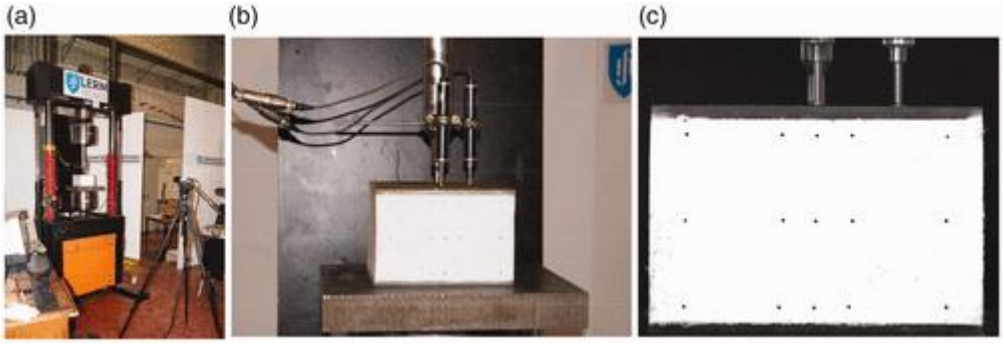

Figure 3. QS indentation tests setup: (a) overview, (b) instrumented specimen and (c) video-extensometer capture.

To confirm that only localised deformation occurred, the deformations of the panel edges were monitored in selected specimens with a video-extensometer (Sony XCG-5005Ehigh-definition camera with a Fujinon Fujifilm HF50SA-1lens). Measurement patterns comprising 15 target points were marked on the front-facing side of the panels (Figures 3(c) and 4(a) and (b)) and their displacements were monitored throughout the tests.

2.2.2 Low-velocity impact tests

The impact tests were carried out using a Rosand IFW5instrumented drop weight machine (Figure 5(a)). Specimens (Figure 5(b)) were impacted by a variable mass dropped from a known height and the resulting force measured by an extremely rigid 'washer' type 60 kN Kistler 9031A load cell (specifically designed for measuring highly dynamic forces) between impact mass and indenter (Figure 5(c)). A metal flag of accurately known height attached to the falling weight gave the incident velocity as it passed through an optical gate, allowing integration of the force versus time data to also give displacement and absorbed energy values.

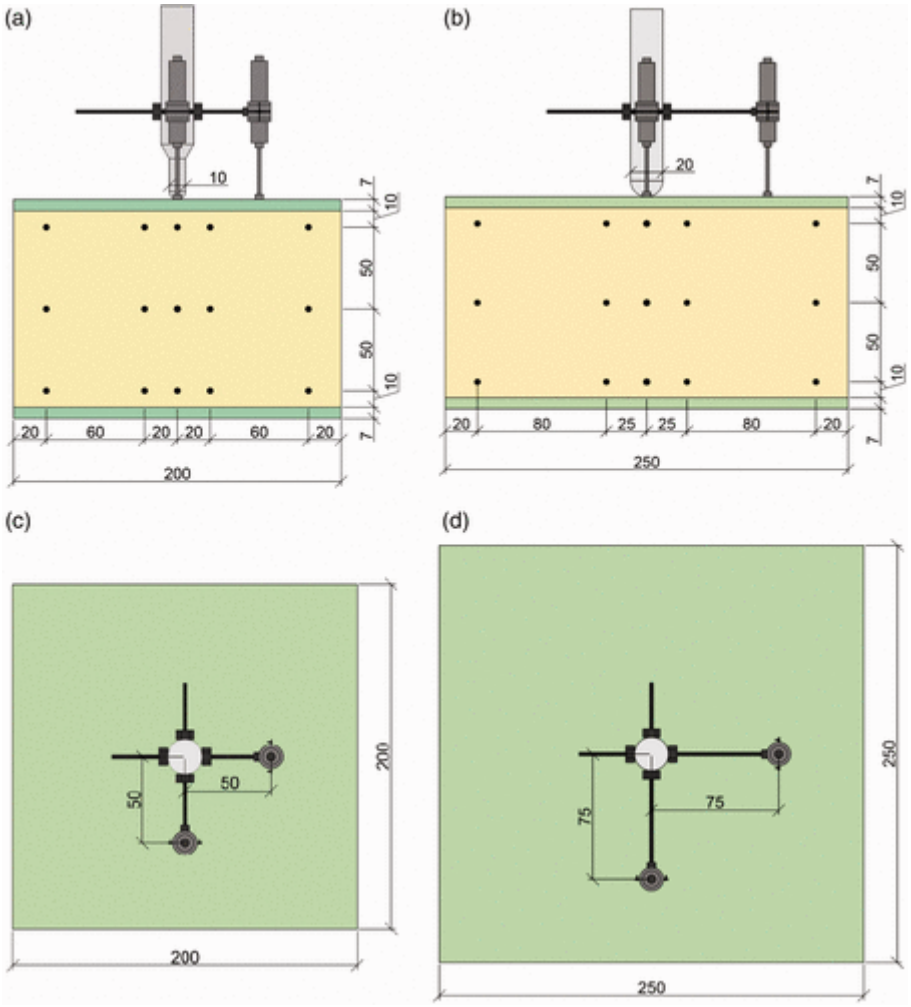

Figure 4. Dimensions and instrumentation for the QS indentation tests: (a) 200 mm specimens front view, (b) 250 mm specimen front view, (c) 200 mm specimens top view and (d) 250 mm specimen top view.

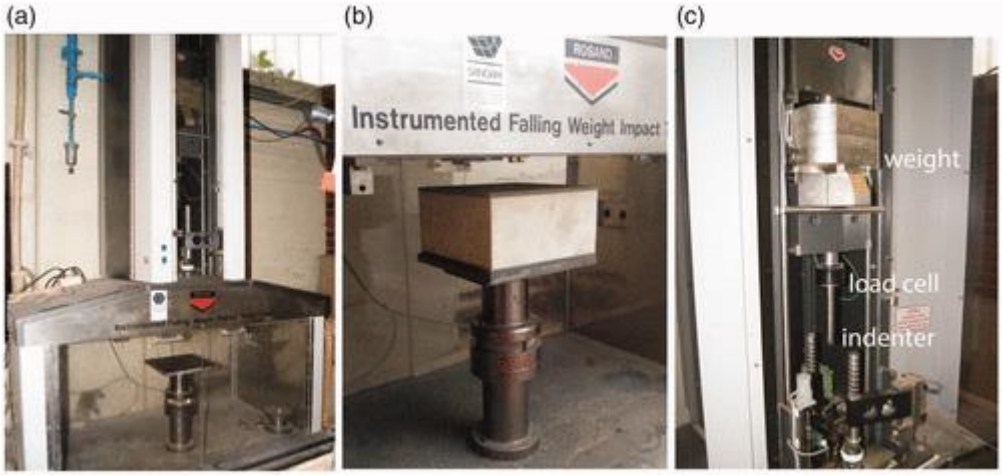

Figure 5. Low-velocity impact tests setup: (a) drop weight machine, (b) test specimen and (c) detail of the test setup.

2.3 Experimental programme

Specimens were fully supported by a rigid 50 mm thick steel plate (Figure 5(b)). Since these thick laminates will not deflect significantly in-service under concentrated impact loadings, this is a relevant boundary condition. This also facilitated ensuring the equality between QS and impact tests required to allow valid comparisons between the two types of tests to be made.

Initially, in order to ensure both that specimen dimensions were large enough to avoid global crushing of the core or bending failure of the faces and that only localised damage was induced, a preliminary QS indentation assessment was carried out on specimens of various dimensions, each with a 1:1 aspect ratio of length to width, for each indenter.

This resulted in the selection of a specimen size of 200 mm × 200 mm, with the exception of PUR specimens for all impact tests and for QS tests with 20 and 30 mm hemispherical and flat indenters, which required specimens of 250 mm × 250 mm to avoid invalid failure modes (Figure 4, Tables 3 and 4).

Type of core	Specimen dimensions (mm)	Indenter type	No. of tests
PUR	200 × 200	10H	2
		10F	2
	250 × 250	20H	2
		20F	1
		30H	2
PET	200 × 200	10H	1
		10F	1
		20H	1
		20F	1
BAL	200 × 200	10H	1
		10F	2

BAL: balsa; PET: polyethylene terephthalate; PUR: polyurethane.

Table 3. Summary of quasi-static indentation tests.

Type of core	Specimen dimensions (mm)	Indenter type	No. of tests
PUR	250 × 250	10H	3
		10F	2
		20H	2
PET	200 × 200	10H	3
		10F	3
		20H	2
BAL	200 × 200	10H	3
		10F	3

BAL: balsa; PET: polyethylene terephthalate; PUR: polyurethane.

Table 4. Summary of low-velocity impact tests.

The QS tests of Table 3 were then completed under the test conditions detailed in 'QS indentation tests' section. The test speed of 2 mm/min was selected to ensure no dynamic effects were present and to give a large order of magnitude difference in loading rates between QS and impact tests, whilst giving a practically manageable test duration. Tests were continued after full perforation of the upper face laminate and significant penetration of the core, but were stopped well before contact with the lower face to avoid damage to the test equipment (due to the fully supported boundary condition used).

Regarding the impact tests, in order to both ensure significant impact damage was seen and to avoid destruction of the fragile dynamic load cell of the machine, a target incident kinetic energy (IKE) was set as that which would give similar damage as seen in the QS tests, i.e. total perforation of the upper face laminate (hereby referred to simply as 'perforation'), whilst avoiding total penetration of the core resulting in contact with the fully supported lower face. Prediction of the required IKE for a given amount of damage is very problematic, but previous research [10,27,28] has shown that QS behaviour is a good predictor of impact behaviour up to initial damage and that post-damage impact behaviour may be predicted using an empirically obtained 'dynamic scaling factor'. Hence, estimates of the amount of IKE required for impacted face penetration were made by multiplying the relevant QS energies by dynamic scaling factors of 2.00 and 2.75 for the foam and BAL-cored sandwiches, respectively. These dynamic scaling factors values were modified from those previously empirically obtained for comparable, but slightly less robust, laminates [10,28] to try to conservatively ensure full perforation.

Since these scaling factors were only expected to give estimates of the IKE for perforation, a preliminary round of impact tests was first conducted to refine the IKEs required for each panel–indenter combination. The severity of an impact event is proportional to the IKE, but for drop weight testing this energy may be obtained by a large range of combinations of impact mass and drop height. However, differences in behaviour due to the range of impact loading rates obtainable at the same IKE for the range of drop heights available with this type of machine (in this case up to 2 m) are not detectable [14]. Hence, in order to keep impact velocities constant a drop height of 0.75 m was used for these preliminary impact tests, whilst varying the impact mass to achieve the required IKE. This specific drop height was selected since it is large enough to avoid significant errors due to measurement of drop height and friction, and also allowed the selection of all required IKEs with the available impact masses.

In most cases, the estimated perforation IKE did in fact give specimen perforation. However, when a test at the estimated perforation IKE did not result in full penetration, the test was repeated at a higher IKE obtained by increasing the drop height until full penetration was achieved. Although the estimated penetration IKE of the PUR laminate with a 20 mm flat indenter was only 540 J, the preliminary tests did not result in penetration even with an IKE of over 700 J, and since this is the safe limit IKE of the impact machine, no further tests were carried out for this panel–indenter combination. This led to the decision not to proceed with any impact tests using the 20 mm flat and 30 mm hemispherical indenters (which were used in the QS tests). Then, once the perforation IKEs had been established, further replications of

tests of specimens of each indenter-panel combination were made in a concluding round of tests.

Summaries of the performed QS indentation and impact tests are given in Tables 3 and 4, respectively, including the type of core material, the indenter characteristics, the specimen dimensions and the number of replicate specimens for each condition (this number was limited by the material available for the test programme; yet, replicate specimens provided consistent results). Further details of the impact tests, such as drop height and impact mass, are provided in the next section.

3 Results and discussion

3.1 QS indentation

Figure 6 presents representative curves of the QS indentation load versus indenter displacement (i.e. cross-head displacement given by the test machine) for each indenter, grouped by panel type/core material. All of the obtained curves exhibited an approximately linear initial segment. The slopes of the initial segments were relatively similar for all curves of each panel type, independently of indenter shape or diameter. This indicates that indentation stiffness of the tested panels is relatively unaffected by the indenter characteristics within the range of indenters used and for the type of panels analysed here.

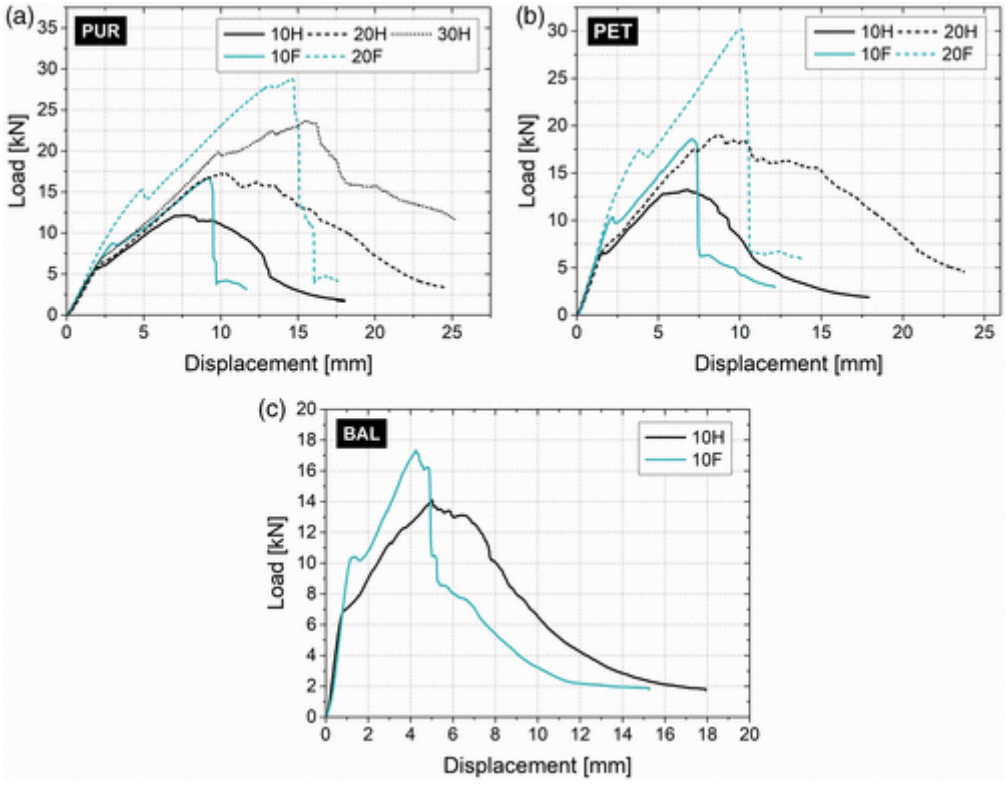

Figure 6. QS indentation results: (a) PUR, (b) PET and (c) BAL panels.

No significant damage to the panels was observed during this initial stage; however, faint cracking sounds were audible for loads between 2.8 and 5.0 kN, which may be assumed to have been caused by micro-cracking of the resin matrix.

The approximately linear initial stage of the load versus displacement behaviour ended as the first visible damage to the specimens occurred. This damage corresponded to stiffness reduction for all indenters, with a sudden force drop visible only for the flat indenters. Damage was characterised by the appearance of a region of whitening around the contact area between the indenter and the specimen (Figure 7), which was presumably due to delamination of the face laminate.

Figure 7. Damage induced in the QS indentation tests: (a) hemispherical indenters, (b) flat indenters and (c) hemispherical indenter (10H) in a BAL specimen.

After this first damage (FD) the load again increased until the onset of the perforation process (represented in the plot by the peak load in each curve), after which a progressive or sudden force decrease was seen for the hemispherical and flat indenters, respectively. These differences in perforation load versus displacement behaviour corresponded to the variable contact area of the hemispherical indenters causing progressive damage and shearing of the fibres (Figure 7(a)), whereas in contrast the constant contact area of the flat indenters led to sudden shearing of the fibres (Figure 7(b)). QS perforation behaviour is discussed alongside that of the impact tests in the 'Low velocity impact' section.

The video-extensometer measurements did not capture any significant deformation of the lateral faces of the specimens throughout the duration of the tests, confirming that the adopted specimen geometries were adequate and that only localised damage was induced.

A summary of the main results obtained from the QS indentation tests is shown in Table 5 and in Figure 8. In these, Kis the stiffness calculated in the initial linear segment of the load versus deflection curves; dFDand dpeakare the indenter (cross-head) displacements at the points of FD and peak load, respectively; FFDand Fpeak, and AEFDand AEpeakare the load and absorbed energy, respectively, at those same points. The absorbed energy values were estimated based on the integration of the area beneath the indentation load versus displacement curves up to each notable point. These absorbed energy values include both elastic and non-elastic behaviours since both are valid energy absorption mechanisms. Further investigation exploring the distribution of this total absorbed energy between reversibly (elastic) and irreversibly (non-elastic, due to damage mechanisms) absorbed energies at varying levels of damage would be of interest, but this was beyond the scope of the present study. In any case, for the most severe case of full penetration which is of most interest here any initial elastically absorbed energy is eventually absorbed by damage mechanisms.

Panel	Indenter	K (kN/mm)	d_{FD} (mm)	d_{peak} (mm)	F_{FD} (kN)	F_{peak} (kN)	AE_{FD} (J)	AE_{peak} (J)
PUR	10H	3.3	1.8	7.6	5.5	12.2	5.3	57.8
	10F	3.4	3.0	9.3	8.7	16.8	13.3	91.4
	20H	3.3	2.3	10.0	6.4	17.3	7.0	99.8
	20F	3.9	4.9	14.7	15.3	28.8	41.9	258.1
	30H	3.6	2.3	15.5	6.8	23.6	7.6	227.9
PET	10H	5.4	1.3	6.8	6.3	13.2	4.1	60.6
	10F	5.8	2.2	7.1	10.3	18.6	11.4	79.5
	20H	4.8	1.7	8.8	7.3	19.0	6.1	101.8
	20F	5.3	3.9	10.1	17.5	30.2	38.6	181.7
BAL	10H	9.7	0.9	5.2	6.6	14.3	3.0	49.4
	10F	9.5	1.3	4.3	10.4	17.3	7.2	46.0

BAL: balsa; PET: polyethylene terephthalate; PUR: polyurethane.

Table 5. Summary of results from the quasi-static indentation tests (average values are given where more than one specimen was tested, cf. Table 3).

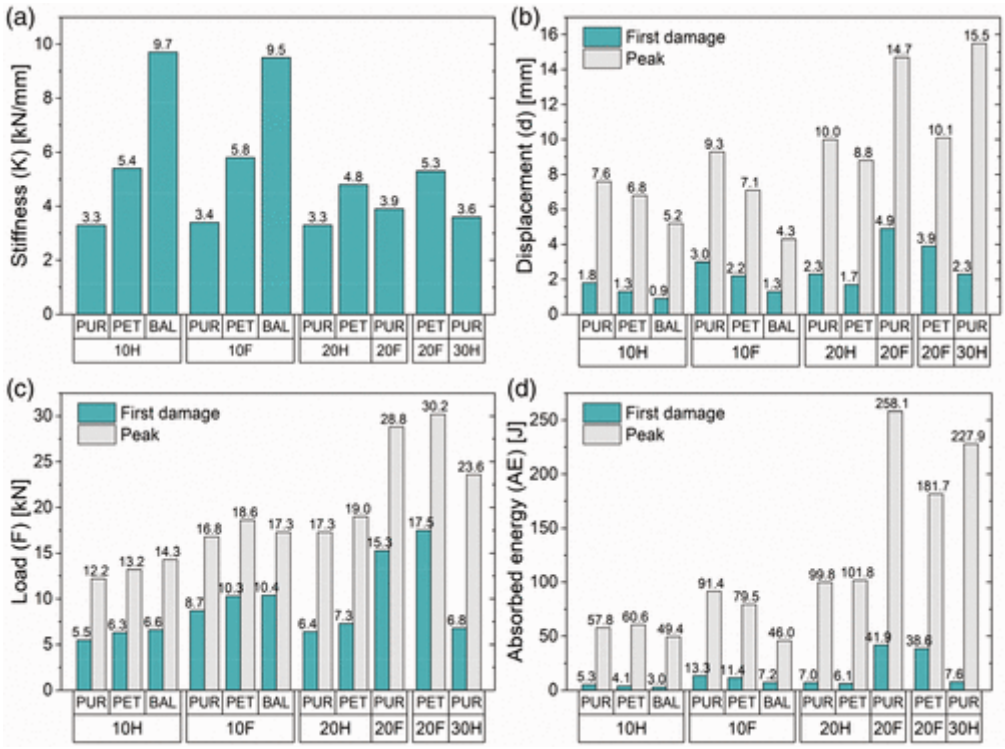

Figure 8. Summary QS indentation results: (a) stiffness, (b) displacement, (c) load and (d) absorbed energy. BAL: balsa; PET: polyethylene terephthalate; PUR: polyurethane.

As a general note, the FD load values obtained here are comfortably high compared to the localised static actions that can be reasonably expected to occur during service for most civil engineering applications. The critical scenarios should result mostly from accidental low-velocity impact events, which will be further discussed in 'Comparison with QS results' section.

As mentioned above, the indentation stiffness (K) was relatively unaffected by the type of indenter. However, the FD and peak displacements (dFD, dpeak), loads (FFD, Fpeak) and absorbed energies (EFD, Epeak) varied significantly with indenter characteristics, generally increasing with indenter diameter and being higher for flat indenters compared to hemispherical ones. In fact, independently of core material, the load and displacement values

at FD were consistently about 60% higher with flat versus hemispherical indenters for the 10 mm case. This difference was of about 130% for 20 mm indenters. The values of absorbed energy at FD were, on average, about 150% higher for flat indenters compared to hemispherical ones of the 10 mm diameter, and about 500% higher for the 20 mm indenters. The peak loads, displacements and absorbed energies had a less consistent dependency of indenter shape, but still followed the same general trend.

Regarding the influence of core material, and taking the PUR panel results as reference, the indentation stiffness of the PET and BAL panels was, respectively, about 54 and 187% higher (on average, for all indenters) than that shown by those panels. This result is logical and consistent with the relative stiffness of the three core materials. This resulted in lower displacements at FD and peak for the stiffer cored panels. On the other hand, the FD and peak resistance values of the PET panels were, on average, 15 and 8% higher than in the PUR panels. For the BAL panels, such figures were 20 and 10%, respectively. The higher deformability of the PUR panels translated to the highest energy absorption capacity among the three types of panels. In fact, the energy absorbed up to FD by the PET and BAL panels was, on average, 14 and 45% lower than that of the PUR panels. These figures were 9 and 32% considering absorbed energy up to the panels' peak resistance.

These results are illustrated in Figure 9, which presents representative indentation load versus displacement curves for the 10 mm flat (Figure 9(a)) and hemispherical (Figure 9(b)) indenters for the three core materials.

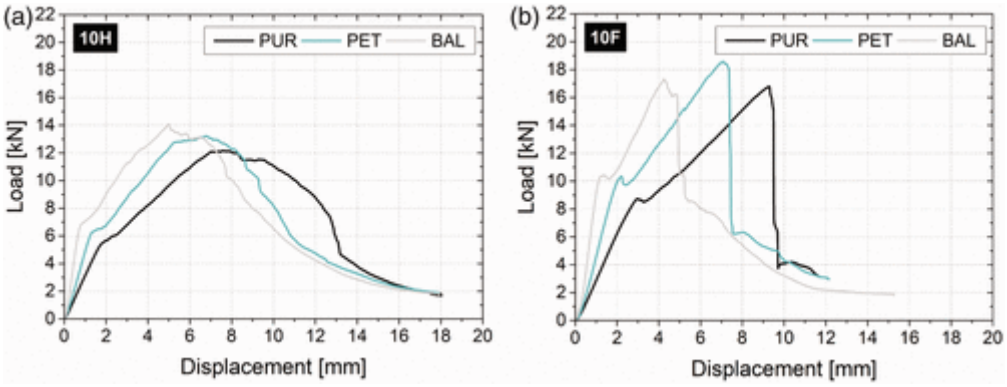

Figure 9. QS indentation results: (a) 10H indenter and (b) 10F indenter. BAL: balsa; PET: polyethylene terephthalate; PUR: polyurethane.

Another key difference that was observed between panels of different core material pertained to their failure modes, namely the formation of cracks along the transverse and longitudinal fibre directions of the facings, as may be observed in Figure 7(a) and (b). Such cracks were observed in the PUR and PET panels, propagating outwards from the contact area between the indenter and the facing. In the BAL panels, such cracks were not observed (Figure 7(c)), which is an indication of the higher degree of damage concentration and less pronounced bending of the facings in those panels compared to the former; this lower bending deformability of the facings should be ascribed to the higher stiffness of BAL compared to the foams.

The previous observation is supported by the measurements obtained with the displacement transducers installed along the longitudinal and transverse fibre directions of the facings. The

longitudinal direction measurements for the FD and peak loading points are shown in Figure 10, considering the different types of core material and the 10 mm hemispherical and flat indenters (the plots assume symmetrical deformations; the data points were connected with straight lines for the sake of legibility). The deformations measured 50 mm away from the loading point in the BAL panels were significantly lower than those measured for the polymeric foam cored panels, especially for the hemispherical indenter, and showed only negligible increments between the moments of FD and peak load.

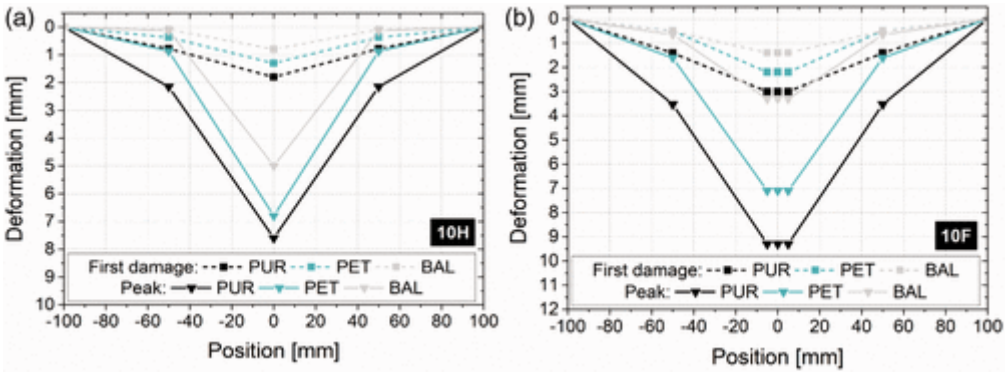

Figure 10. Displacement transducer measurements along the longitudinal (main) fibre direction of the facings at FD and peak loads: (a) 10H indenter and (b) 10F indenter. BAL: balsa; PET: polyethylene terephthalate; PUR: polyurethane.

The displacements measured along the longitudinal direction of the laminates were typically higher than those in the transverse direction, independently of indenter type, due to the higher reinforcement content along the main fibre direction.

3.2 Low velocity impact

In this section, the impact test results are first explained and presented, then comparisons are made with the equivalent QS results, and finally the effects of indenter geometry and core material are discussed. The failure modes seen in the impact tests were the same as those shown in Figure 7 for the QS tests and discussed in the previous section.

3.2.1 Impact results

Dynamic impact testing of composite materials results in a raw force versus displacement response which is superimposed with oscillations due both to unwanted vibrations (of the machine structure, for example) and due to vibrations around the contact stiffness [30]. Although the latter of these two types of oscillations is actually a form of material response, since the structural behaviour and damage of the laminates is of interest here, appropriate filtering (which removes oscillation whilst leaving the form of the impact response intact) is required. For this specific case, a moving average filter with a window of five data points (sampled at 20 kHz) was found to achieve the best balance of this, as illustrated in Figure 11.

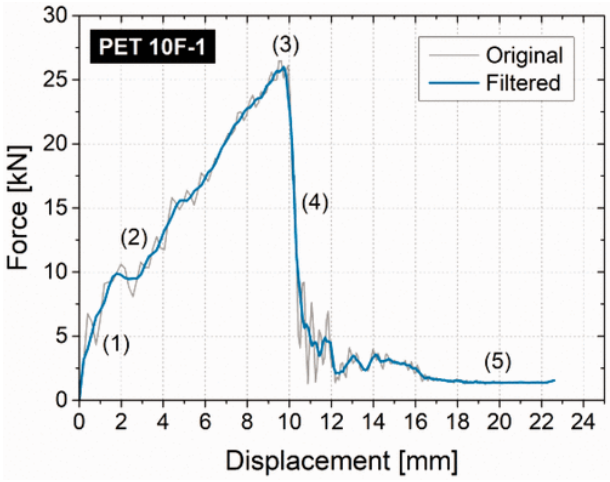

Figure 11. Illustrative raw and filtered impact test force versus displacement behaviour. PET: polyethylene terephthalate.

As well as the force versus displacement response, the amount of energy absorbed by the target laminate during the impact event is also of interest, and hence the filtered impact force and absorbed energy results are plotted against contact point displacement for all tests in Figure 12. This figure also includes the equivalent QS responses for comparative purposes.

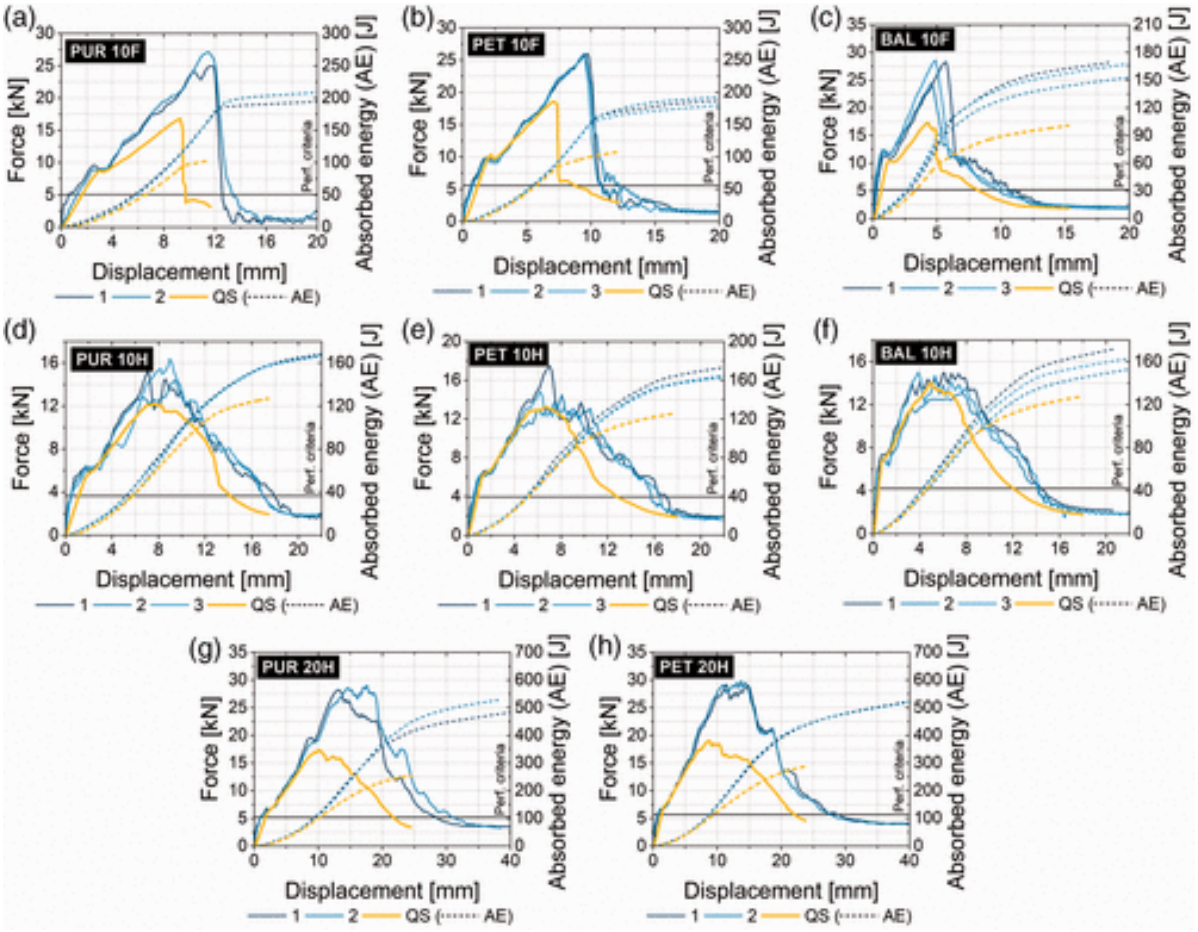

Figure 12. Impact responses (including comparison with QS results, QS): (a) PUR 10F, (b) PET 10F, (c) BAL 10F, (d) PUR 10H, (e) PET 10H, (f) BAL 10H, (g) PUR 20H and (h) PET 20H. AE: absorbed energy; QS: quasi-static.

The salient points or stages of the typical impact behaviour seen in these plots are as follows:

1. an initial undamaged response;
2. a sudden reduction in stiffness (often accompanied by a small drop in load) due to initial damage;
3. the initiation of perforation as maximum load is approached;
4. a drop in load as perforation progresses (sudden drop for flat indenters, more progressive for hemi-spherical);
5. a plateauing of the load after full perforation due to friction as the cylindrical impactor continues to pass through the perforation.

Hence, the values of force (F), displacement (d) and absorbed energy (AE) at maximum force and perforation (subscripts 'max'/'Fmax' and 'perf') are presented in Table 6, along with the incident velocity registered in each impact test (Vincident). As will be discussed in the 'Comparison with QS results' section, the initial stiffness and point of initial damage are not accurately retrievable from the impact results and are therefore not presented.

In fact, the appropriate definition of perforation here is by no means as straightforward as its linguistic equivalent ('to make a hole through something') would suggest. It is impractical to try to identify accurately the point at which a hole appears in the impacted specimen, and in this case we are interested in when fullperforation occurs (i.e. when the impactor passes right through the laminated skin). Stage 5 of the impact behaviour described above shows that full perforation has occurred when the load reduces to a level value, but the approach to this is asymptotical, subject to fluctuations and significantly inconstant due to the severe laminate damage seen. Hence, after consideration of various criteria, the point at which the load dropped to a value of 30% of the peak QS load was selected as a definition of 'full perforation', which both occurred consistently close to the beginning of the perforated load plateau of stage 5 above (as can be seen in Figure 12, horizontal lines marked 'Perf. Criteria') and allowed accurate and objective measurements to be made.

3.2.2 Comparison with QS results

It was not possible to completely remove the effects of the stronger contact stiffness oscillations in the initial impact responses (see Figure 11) without significantly distorting the rest of the response. Hence this first part of the impact response is difficult to interpret accurately and so Table 6 contains neither values concerning initial impact stiffness nor the point at which FD occurs. Despite this, the plots of Figure 12 do indicate that this 'obscured' underlying initial impact behaviour appears to be very similar to the much clearer QS initial response, and therefore QS testing appears to be both a more accurate and an easier method of estimating the impact initial stiffness and point of first impact, as previously proposed in Sutherland and Guedes Soares [27]. However, the fact that initial stiffness in almost all of the plots of Figure 12 is higher for impact than for QS loading could still be due to a loading-rate ('strain-rate') effect to some degree, but in order to be able to investigate this possibility further, more advanced filtering methods would have to be explored, and data with a significantly higher sample rate would be required.

Core	Indenter	Test	$V_{incident}$ (m/s)	Mass (kg)	IKE (J)	Max. force values			Perforation values		
						F_{max} (kN)	d_{Fmax} (mm)	AE_{Fmax} (J)	F_{perf} (kN)	d_{perf} (mm)	AE_{perf} (J)
PUR	10F	QS	(–)	(–)	(–)	16.80	9.3	91	5.04	9.7	96
		Impact 1	3.95	25.3	197	24.96	11.8	173	(–)	12.6	186
		Impact 2	4.25	35.3	319	27.15	11.4	164	(–)	13.4	197
		Increase from static to impact				**55%**	**25%**	**84%**	(–)	**34%**	**99%**
PET	10F	QS	(–)	(–)	(–)	18.59	7.1	79	5.58	8.7	94
		Impact 1	4.00	25.3	202	25.99	9.7	148	(–)	10.9	165
		Impact 2	3.90	30.3	231	25.97	9.5	141	(–)	12.2	174
		Impact 3	3.95	30.3	236	25.42	9.3	137	(–)	10.8	158
		Increase from static to impact				**39%**	**34%**	**78%**	(–)	**30%**	**77%**
BAL	10F	QS	(–)	(–)	(–)	17.32	4.3	46	5.20	8.1	81
		Impact 1	3.79	25.3	182	28.28	5.7	97	(–)	10.5	147
		Impact 2	3.88	30.3	228	24.47	4.5	71	(–)	9.7	127
		Impact 3	4.02	30.3	245	28.55	4.9	84	(–)	10.2	142
		Increase from static to impact				**56%**	**18%**	**82%**	(–)	**25%**	**71%**
PUR	10H	QS	(–)	(–)	(–)	12.16	7.6	58	3.65	14.1	118
		Impact 1	4.02	30.3	245	15.31	7.1	61	(–)	18.0	160
		Impact 2	3.95	30.3	236	14.38	9.4	90	(–)	17.0	156
		Impact 3	3.36	30.3	171	16.36	8.9	82	(–)	17.0	156
		Increase from static to impact				**26%**	**12%**	**35%**	(–)	**23%**	**33%**
PET	10H	QS	(–)	(–)	(–)	13.22	6.8	61	3.97	12.8	112
		Impact 1	3.69	30.3	206	17.44	7.1	71	(–)	17.0	162
		Impact 2	3.86	30.3	226	14.48	8.1	77	(–)	15.8	151
		Impact 3	3.95	30.3	236	14.81	6.2	56	(–)	16.5	152
		Increase from static to impact				**18%**	**5%**	**12%**	(–)	**28%**	**38%**
BAL	10H	QS	(–)	(–)	(–)	14.08	5.0	48	4.23	12.0	112
		Impact 1	3.63	35.3	233	14.95	6.1	69	(–)	14.4	155
		Impact 2	3.84	30.3	223	13.05	7.6	78	(–)	14.2	135
		Impact 3	3.97	30.3	239	15.00	3.9	36	(–)	14.3	146
		Increase from static to impact				**2%**	**17%**	**28%**	(–)	**19%**	**30%**
PUR	20H	QS	(–)	(–)	(–)	17.26	10.0	100	5.18	21.7	242
		Impact 1	4.25	55.3	500	28.21	13.2	196	(–)	28.5	440
		Impact 2	4.31	55.3	513	28.99	17.6	310	(–)	31.0	499
		Increase from static to impact				**66%**	**55%**	**153%**	(–)	**37%**	**94%**
PET	20H	QS	(–)	(–)	(–)	19.01	8.8	102	5.70	22.1	279
		Impact 1	4.00	75.3	602	29.13	11.3	182	(–)	28.9	474
		Impact 2	4.00	75.3	602	29.83	13.7	256	(–)	27.6	466
		Increase from static to impact				**55%**	**43%**	**115%**	(–)	**28%**	**68%**

BAL: balsa; IKE: incident kinetic energy; PET: polyethylene terephthalate; PUR: polyurethane.

Table 6. Summary of impact results and comparison with quasi-static (QS) results.

In fact, the QS and impact responses are also very similar as the load climbs with a reduced stiffness response after the initiation of FD, for all cases except for PUR and BAL cored laminates impacted with the 10mm diameter flat-ended indenter (10F), where QS stiffness is

more severely decreased than is the dynamic impact stiffness. The reasons for these two exceptions are not at all clear and require further investigation.

Figure 12 and the bold maximum force percentage figures in Table 6 indicate that the maximum force (indicating the start of perforation) for all laminates impacted with flat-ended 10 mm (10F) and hemispherical 20 mm (20H) indenters is significantly higher for impact than for QS tests (by between approximately 40 and 65%). Similar behaviour, thought to stem from a lack of time for damage propagation in the exceedingly faster impact tests, was seen in previous studies [10,27,28].

However, as further clarified in Figure 13, this dynamic effect is much weaker for the 10 mm diameter hemispherical indenter (10H), and for this indenter with the BAL cored laminate there is no dynamic effect at all; static and impact maximum values differ by only 2% (Table 6). These trends in maximum force are naturally also seen in the associated absorbed energy at maximum force results (Figure 14).

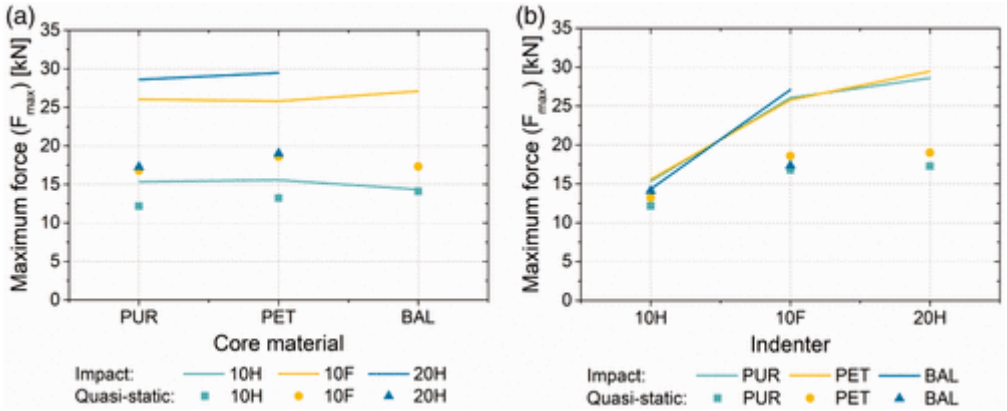

Figure 13. Maximum force w.r.t. (a) core and (b) indenter geometry. BAL: balsa; PET: polyethylene terephthalate; PUR: polyurethane.

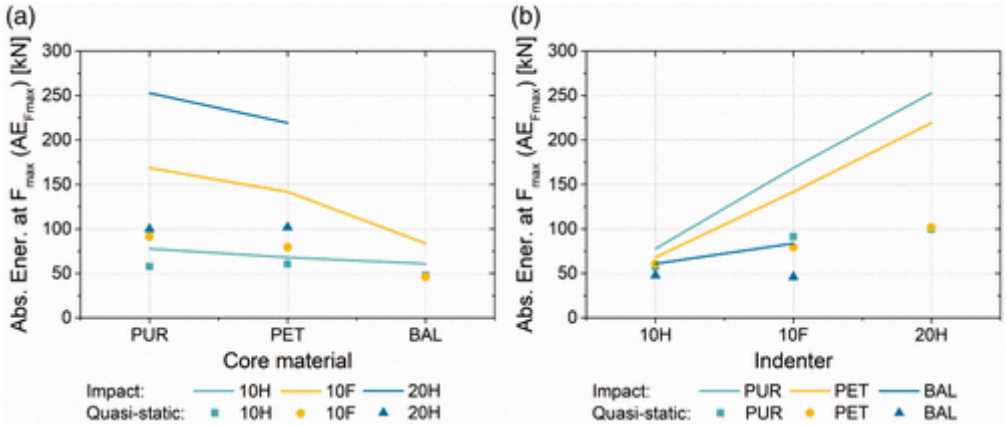

Figure 14. Absorbed energy at maximum force w.r.t. (a) core and (b) indenter geometry. BAL: balsa; PET: polyethylene terephthalate; PUR: polyurethane.

Similarly, Figure 15 shows perforation to require more energy for dynamic impact tests than for QS ones, and Table 6 shows that for all laminates impacted with flat-ended 10 mm (10F) and hemispherical 20 mm (20H) indenters this increase is even more significant, at between approximately 70 and 100%. Again, this dynamic effect is not as strong (an increase of between

approximately 30 and 40%) for the 10 mm diameter hemispherical (10H) indenter, as clarified in Figure 15, but in this case is not weaker for the BAL core, as it was for maximum force and AE at maximum force.

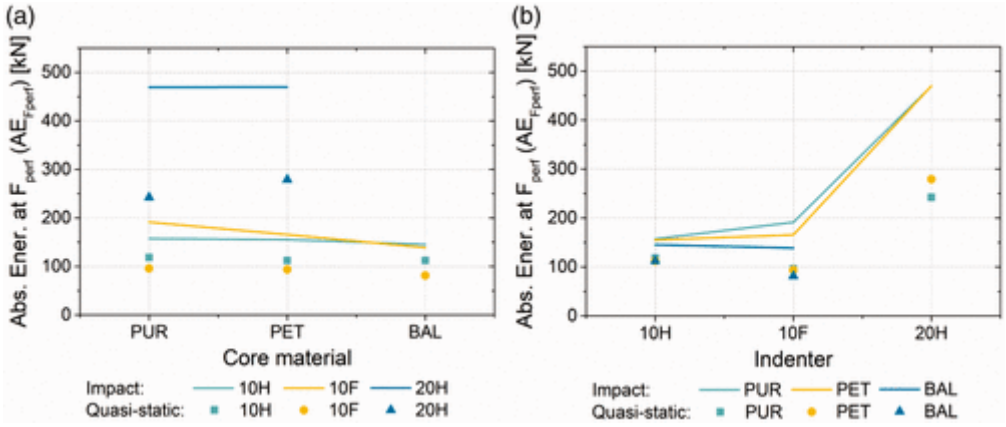

Figure 15. Absorbed energy at perforation w.r.t. (a) core and (b) indenter geometry. BAL: balsa; PET: polyethylene terephthalate; PUR: polyurethane.

The reason(s) for the difference in behaviour of the 10 mm hemispherical indenter is(are) not at all clear from the data available from this study, but are probably due to differences in the failure modes and mechanisms occurring in each case and require further investigation.

Finally, despite the much higher velocities involved, there appears to be little difference between the average QS and impact final perforated plateau load values (on average approximately 2.5 and 2.0 kN, respectively) as the cylindrical indenter continues to pass through the perforated laminate upper skin and into the core below.

Given the wide range of possible static loadings and impact events and severities possible, it is not possible to generalise as to whether these laminates are sufficiently resistant to such loads. However, in order to put the obtained values into some context, it is illustrative to consider some typical values of foreseeable localised actions on relevant civil engineering structures (e.g. pedestrian loads on bridge decks, furniture supports or falling objects on building floors). Taking into account the discussion above, if one considers QS results as representative of the initial impact response of the panels, for the materials and geometries tested the observed FD loads (e.g. 5.5 kN for the PUR 10H case, which is the most critical scenario, cf. Table 5) offer a fairly comfortable safety margin. For example, taking the values discussed in Sutherland et al. [11]: a pedestrian of 75 kg walking at a normal pace of two steps per second typically exerts a force of approximately 1 kN; this force may be of over 2 kN whilst running at four steps per second. The FD loads presented in Table 5 provide a fairly comfortable margin as compared to these illustrative values.

3.2.3 Effects of core and indenter geometry

The effects of core and indenter geometry on the change in behaviour between QS and impact tests have been discussed in the previous section; here their effects on the impact behaviours seen are discussed.

In terms of impact maximum force, the effect of core material seen in Figure 13(a) is small, although Figure 14(a) shows a decreasing trend from PUR through PET to BAL for the energy

absorbed up to maximum force, indicating that the foam cored laminates generally resisted better the onset of perforation.

An increasing trend for both impact maximum force and impact AE to maximum force with a change in indenter from 10H through 10F to 20H is evident in Figures 13(b) and 14(b) and is no doubt due to the increasingly extensive and severe damage incurred by the use of larger and flatter indenters.

Figure 15(a) shows that the energy required to totally perforate the laminates does not appear to significantly change between the different core materials, except for the flat 10mm diameter (10H) indenter where PUR is more resistant and BAL is less resistant than PET to perforation. Again, a flat indenter requires more energy to totally perforate the laminate, but the largest effect is seen by doubling the impactor diameter, as seen in Figure 15(b).

The impact perforated plateau load values as the cylindrical indenter continues to pass through the perforated laminate upper skin and into the core below increase with indenter diameter (on average approximately 2 and 4 kN for 10 and 20mm diameter indenters, respectively), but are not particularly sensitive to core material (on average approximately 2.2 kN for both foam cores and 2.0 kN for BAL).

4 Analytical modelling

4.1 Overview and objectives

To consider the indentation and impact phenomena in the design of relatively thick sandwich panels designed for use in civil and ocean engineering structures, the appropriate analytical tools for their strength prediction under those actions must be validated. In the context of civil engineering, closed-form equations are typically favoured in design practice. Accordingly, two closed-form expressions for the prediction of FD indentation load were assessed in this study, stemming from the analytical models proposed by Wen et al. [26] for flat indenters and by Olsson [25] for hemispherical indenters, as described in the following sections. These were applied to the sandwich panels and materials considered here, and the FD load estimates were compared to the respective experimental data.

4.2 Model description

4.2.1 Wen et al. model

Wen et al. [26] proposed an analytical model to simulate the behaviour of composite sandwich panels with thick faces impacted by flat indenters. According to the authors, for thick faces the membrane effect can be neglected and the FD resistance of the sandwich panels (P_f) is thus given by

$$P_f = 2\pi R h \tau_{13} + K_c \pi R^2 \sigma_{cu} \quad (1)$$

in which R is the indenter radius, h is the face thickness, τ_{13} is the laminate (through-thickness) shear strength, K_c is a constraint factor representing the effect of the core material and σ_{cu} is the core compressive strength in the through-thickness direction. In the previous equation, the first term gives the face laminate contribution and the second the core contribution.

4.2.2 Olsson model

Olsson [25] proposed an analytical model to simulate the behaviour of composite sandwich panels impacted by hemispherical indenters. According to this model, the contribution of the core to the first delamination is neglected and this is assumed to be dependent only on face laminate parameters, namely the bending stiffness of the faces (D_f) and the mode II critical strain energy release rate (G_{IIc}), leading to the following expression for the force at first delamination

$$P_f = \pi \sqrt{\frac{32 D_f G_{IIc}}{3}} \tag{2}$$

4.3 Application to experimental results

4.3.1 Wen et al. model

The face sheet contribution to FD resistance given by the first term of the Wen et al. model assumes that the through-the-thickness shear strength of the facing material is constant along the perimeter of the indentation area. However, unlike metallic face sheets, FRP laminates are typically not isotropic. For the GFRP laminates considered in this study, the interlaminar shear strength value differs significantly between the longitudinal ($\tau_{isu,L}$=37.1 MPa) and transverse ($\tau_{isu,T}$=24.1 MPa) directions of the laminates (cf. Table 2). Using either value constitutes a rough approximation of the laminates' behaviour, providing lower and upper bounds (using the transverse and longitudinal properties, respectively) of the sandwich panels' FD resistance. If one takes the longitudinal direction value, the left-hand term of equation (1) yields a value of 8.16 kN for a 10 mm diameter flat indenter (10F) or 16.32 kN for a 20 mm flat indenter (20F). Taking the transverse direction interlaminar shear strength of the laminates, these values become 5.30 and 10.60 kN, respectively.

Regarding the core contribution to the FD resistance, it is important to note that the constraint factor Kc is an empirical parameter. Reference values for this parameter ($1.7<K_c<2.5$) were presented by Reddy et al. [31] for sandwich panels with metallic faces and various foam cores. However, these sandwich laminates are very different from those studied here, namely by having relatively thin metallic face sheets instead of relatively thick GFRP facings. In order to evaluate the influence of the constraint factor (and of the overall core contribution) to the FD resistance, a parametric study was carried out where different values of K_c (ranging from 0 to 5) were considered. The results are summarised in Figure 16, considering the interlaminar shear strength along the longitudinal direction of the laminates, which gave the best fit to the experimental data.

Setting K_c=0 corresponds to neglecting the core material's contribution to the FD resistance of the panels, resulting in P_f values equal to those discussed above for the contribution of the facings alone. Comparing the predictions with the experimental results, one may observe that (i) overall they are reasonably close to the experimental data, and (ii) the relative contribution of the core materials to the FD resistance is significantly lower when compared to that of the facings, even for the highest values of K_c considered. In fact, for a K_c value of 5 in the PUR 10F case, this contribution amounts to 3% of the predicted FD resistance; this figure is 22% for the

BAL 10F case, showing that, as expected, the relative core contribution increases with the strength of the core material, being higher for the BAL wood cored panels and lower for the foam cores.

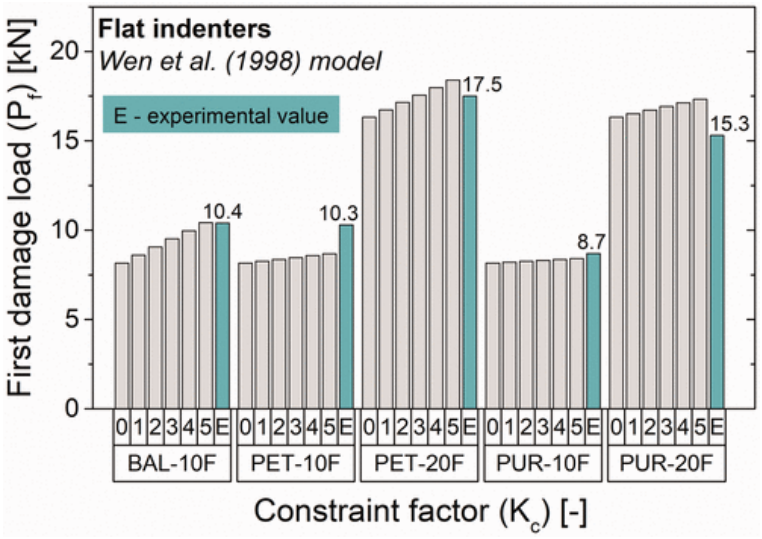

Figure 16. FD load predictions of Wen et al. [26] model for flat indenters with different constraint factor values. BAL: balsa; PET: polyethylene terephthalate; PUR: polyurethane.

However, one may also conclude that it is not possible to calibrate the K_c parameter based on the results presented here, given that inconsistent and unrealistic estimates would be obtained if a model fitting exercise was to be carried out. For example, for the PET-10F case, one would obtain a Kc of over 20, which seems unrealistically high; for the PUR-20F case, such an exercise would lead to a negative value for K_c. This prompts the need (i) for further experimental investigations in order to calibrate this parameter as a function of different materials, geometries and indenter characteristics and (ii) for more advanced analytical models.

Despite this, the model was still able to provide very reasonable FD load predictions. Considering Kc=2 as reference, as proposed in Wen et al. [26], the relative prediction error varied between −9 and 19% for the materials and indenters considered in this study.

4.3.2 Olsson model

Due to the lack of available G_{IIc} values for the face laminates used in this study, the direct use of equation (2) was not possible. Hence, in order to evaluate this model for thick composite sandwich panels, a parametric study was completed varying G_{IIc} between 500 and 2000 J/m2. This interval was adopted based on typical interlaminar mode II critical strain energy release rate values for GFRP laminates (e.g. Korjakin and Fukards [32] and Alizadeh and Guedes Soares [33]). The model predictions as a function of G_{IIc} are plotted in Figure 17 together with horizontal lines representing the experimental FD indentation load values obtained for the different panel types and hemispherical indenters.

Comparing the experimental values with the model predictions, one may observe that the predictions are within the same order of magnitude as the experimental values. However, it is clear that even if reliable estimates of G_{IIc} were available for the laminates under study, equation (2) would still be insufficient to fully predict the FD indentation load for the various

core materials and indenter combinations presented here for the mere fact that it does not consider those variables in its formulation. Indeed, from the plot in Figure 17, one may observe that the increasing trend in FD load with increasing core stiffness and/or strength and increasing indenter diameter cannot be explained by this simple model, which only considers the bending stiffness and the mode II critical strain energy release rate of the facings. Hence, again it is clear that further investigation is still required on this subject.

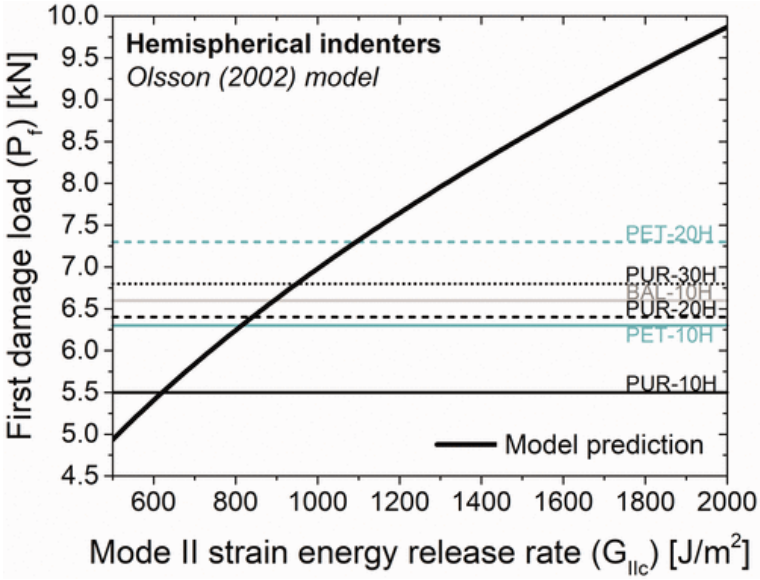

Figure 17. FD load predictions of Olsson [25] model for flat indenters as a function of G_{IIc}. BAL: balsa; PET: polyethylene terephthalate; PUR: polyurethane.

5 Conclusions

The QS indentation and low-velocity impact behaviour of relatively thick sandwich panels designed for civil and ocean engineering structural applications was experimentally studied. Three types of core materials (PUR and PET foams and end-grain BAL) and five different indenters, of varying shape (hemispherical versus flat) and diameter (10, 20 and 30 mm), were considered. The panels were tested in a fully supported configuration, thus eliminating the effects of global panel deflection. Additionally, the predictions of FD resistance given by the analytical models of Wen et al. [26] (for flat indenters) and Olsson [25] (for hemispherical ones) were assessed against the gathered experimental data. The main conclusions drawn from this study are as follows:

- the development of the QS indentation load versus displacement was generally similar between the different core materials and indenters; the FD observed was attributed to the through-thickness delamination of the face laminate and was followed by stiffness reduction; subsequently, the load increased once more until the onset of the perforation process (at peak load), after which a progressive or sudden force decrease, associated with the different failure mechanisms, was seen for the hemispherical and flat indenters, respectively;
- overall, the main stages of the force versus displacement curve in low velocity impact were similar to those seen for QS indentation; in fact, the initial impact behaviour

appears to be very similar to the much clearer QS initial response, suggesting that QS testing may be both a more accurate and an easier method of estimating the low-velocity impact initial stiffness and FD load;

- the indentation stiffness of the tested panels was relatively unaffected by the indenter characteristics within the range of indenters and panels used, but the FD and peak displacements, loads and absorbed energies varied significantly with indenter characteristics, generally increasing with indenter diameter and being higher for flat indenters compared to hemispherical ones;
- regarding core material, the indentation stiffness of the PET and BAL panels was, respectively, about 54 and 187% higher (on average, for all indenters) than that shown by the PUR panels; the FD and peak resistance values of the PET panels were, on average, 15 and 8% higher than in the PUR panels; for the BAL panels, these figures were 20 and 10%, respectively; the higher deformability of the PUR panels translated to the highest energy absorption capacity among the three types of panel;
- generally, perforation required more energy for dynamic impact tests than for QS ones, namely between 30 and 100% more, with differences within this range mainly depending on indenter geometry (higher differences for flat and larger indenters); the effect of core material on the energy required for perforation was less marked, but a slight decreasing trend from PUR through PET to BAL was observed indicating that the foam cored laminates generally resisted better the onset of perforation;
- the Wen et al. [26] model for flat indenters provided reasonably close predictions of FD resistance when compared to the experimental data; furthermore, the relative contribution of the core materials to this resistance was significantly lower when compared to that of the facings; however, there is a need for (i) further experimental investigations in order to calibrate the Kcparameter that accounts for the core material contribution to FD resistance, namely for different materials, panel geometries and indenter characteristics, and (ii) more advanced analytical models;
- the Olsson [25] model for hemispherical indenters provided predictions that are within the same order of magnitude as the experimental values; however, the effects of core material and indenter diameter (which were definitely non-negligible) are not considered in this model, which also prompts the need for further investigation on this subject.

The results of this study thus provided useful insights into the phenomena associated with QS indentation and low velocity impact in thick sandwich panels designed for civil and ocean engineering structural applications, reporting (i) experimental data in terms of damage evolution mechanisms, resistance and energy absorption capabilities of the panels, and how these are influenced by core material properties and indenter characteristics, and (ii) the applicability and limitations of analytical models found in the literature for the prediction of FD loads in such scenarios, envisaging the possibility of their use for the design of sandwich panels under point loads.

References

[1] Correia, J.R., Garrido, M., Gonilha, J.A., Branco, F.A., Reis, L.G. (2012). "GFRP sandwich panels with PU foam and PP honeycomb cores for civil engineering structural applications: Effects of introducing strengthening ribs", International Journal of Structural Integrity, 3(2), 127-147.

[2] Zenkert, D. (1997). The Handbook of Sandwich Construction. Engineering Materials Advisory Services (EMAS), Worcestershire, UK, 442 p.

[3] Pascual, C., de Castro, J., Schueler, A., Keller, T. (2016). "Integration of dye solar cells in load-bearing translucent glass fiber-reinforced polymer laminates", Journal of Composite Materials, 51(7), 939-953.

[4] Abrate, S. (1991). "Impact on Laminated Composite Materials", Applied Mechanics Reviews, 44(4), 155-190.

[5] Abrate, S. (1997). "Localized impact on sandwich structures with laminated facings", Applied Mechanics Reviews, 50(2), 69-82.

[6] Abrate, S. (1998). Impact on Composite Structures. Cambridge University Press, Cambridge; New York, NY, USA.

[7] Abrate, S. (2011). Impact Engineering of Composite Structures. Springer Science & Business Media, Springer-Verlag Wien, 403 p.

[8] Cantwell, W.J., Morton, J. (1991). "The impact resistance of composite materials – a review", Composites, 22(5), 347-362.

[9] Sutherland, L.S. (2018). "A review of impact testing on marine composite materials: Part I – Marine impacts on marine composites", Composite Structures, 188, 197-208.

[10] Sutherland, L.S., Sá, M.F., Correia, J.R., Guedes Soares, C., Gomes, A., Silvestre, N. (2017). "Impact response of pedestrian bridge multicellular pultruded GFRP deck panels", Composite Structures, 171, 473-485.

[11] Sutherland, L.S., Sá, M.F., Correia, J.R., Guedes Soares, C., Gomes, A., Silvestre, N. (2016). "Quasi-static indentation response of pedestrian bridge multicellular pultruded GFRP deck panels", Construction and Building Materials, 118, 307-318.

[12] Sutherland, L.S. (2018). "A review of impact testing on marine composite materials: Part II – Impact event and material parameters", Composite Structures, 188, 503-511.

[13] Sutherland, L.S., 2018. "A review of impact testing on marine composite materials: Part III - Damage tolerance and durability", Composite Structures, 188, 512-518.

[14] Sutherland, L. S., 2018. "A review of impact testing on marine composite materials: Part IV - Scaling, strain rate and marine-type laminates", Composite Structures, 200, 929-938.

[15] Hildebrand, M. (1996). A comparison of FRP-sandwich penetrating impact test methods, Technical Research Centre of Finland, VTT Publications 281, 33 p.

[16] Muscat–Fenech, C., Cortis, J., Cassar, C. (2014). “Impact damage testing on composite marine sandwich panels. Part 1: Quasi-static indentation”, Journal of Sandwich Structures and Materials, 16, 341-376.

[17] Muscat–Fenech, C., Cortis, J., Cassar, C. (2014). “Impact damage testing on composite marine sandwich panels. Part 2: Instrumented drop weight”, Journal of Sandwich Structures and Materials, 16, 443-480.

[18] Sutherland, L.S., Guedes Soares, C. (2005). “Contact indentation of marine composites”, Composite Structures, 70, 287-294.

[19] Sutherland, L.S., Guedes Soares, C. (2003). “The effects of test parameters on the impact response of glass reinforced plastic using an experimental design approach”, Composites Science and Technology, 63, 1-18.

[20] Aamlid, O. (1995). Oblique impact testing of aluminium and composite panels, Technical Report No. 95–2042, DNV.

[21] Atas, C., Sevim, C. (2010). “On the impact response of sandwich composites with cores of balsa wood and PVC foam”, Composite Structures, 93, 40-48.

[22] Daniel, I.M., Abot, J.L., Schubel, P.M., Luo, J.-J. (2012). “Response and damage tolerance of composite sandwich structures under low velocity impact”, Experimental Mechanics, 52(1), 37-47.

[23] Rizov, V.I. (2006). “Non-linear indentation behaviour of foam core sandwich composite materials - A 2D approach”, Computational Materials Science, 35(2), 107-115.

[24] Foo, C.C., Chai, G.B., Seah L.K. (2008). “A model to predict low-velocity impact response and damage in sandwich composites”, Composites Science and Technology, 68(6), 1348-1356.

[25] Olsson R. (2002). “Engineering method for prediction of impact response and damage in sandwich panels”, Journal of Sandwich Structures and Materials, 4(1), 2-29.

[26] Wen, H.M., Reddy, T.Y., Reid, S.R., Soden, P.D. (1998). “Indentation, penetration and perforation of composite laminates and sandwich panels under quasi-static and projectile loading”, Key Engineering Materials, 141-143, 501-552.

[27] Sutherland, L.S., Guedes Soares, C. (2012). “The use of quasi-static testing to obtain the low-velocity impact damage resistance of marine GRP laminates”, Composites Part B: Engineering, 43, 1459-1467.

[28] Castilho, T., Sutherland, L.S., Guedes Soares, C. (2015). “Impact resistance of marine sandwich composites”, in Maritime Technology and Engineering – Proceedings of MARTECH 2014: 2nd International Conference on Maritime Technology and Engineering, Taylor & Francis Group, London, UK, pp. 607-618.

[29] Garrido, M. (2016). Composite sandwich panel floors for building rehabilitation, PhD thesis in Civil Engineering, Instituto Superior Técnico, University of Lisbon.

[30] Sutherland, L.S., Guedes Soares, C. (2005). “Impact behaviour of typical marine composite laminates”, Composites Part B: Engineering, 37, 89–100.

[31] T. Reddy, P. Soden, S. Reid, M. Sadighi (1991). “Impact response of thick composite laminates and sandwich panels”, Collaborative Research Program on the Cost-Effective Use of Fibre-Reinforced Composite Offshore, Marintech Research, Phase 1, Report No. CP04.

[32] Korjakin, A., Fukards, R. (1998). “Comparative study of interlaminar fracture toughness of GFRP with different fiber surface treatments”, Polymer Composites, 19(6), 793-806.

[33] Alizadeh, F., Guedes Soares, C. (2019). “Experimental and numerical investigation of the fracture toughness of Glass/Vinylester composite laminates”, European Journal of Mechanics / A Solids, 73, 204-211.